JMEPEG (2009) 18:912–916
DOI: 10.1007/s11665-008-9316-3

1059-9495/$19.00

Mechanical Properties of Die-Cast Magnesium Alloy MRI 230D

Eli Aghion, Nir Moscovitch, and Amir Arnon

(Submitted August 12, 2007; in revised form September 8, 2008)

MRI 230D was specially developed to overcome the high-temperature limitations of conventionally die-cast magnesium alloys. This innovative alloy was primarily developed for the automotive industry, mainly for power-train applications operating under high-temperature conditions. The present article aims at evaluating the die-casting characteristics of MRI 230D in comparison with conventional AZ91D Mg alloy. These characteristics are used to evaluate the applicability of this alloy for die-casting operations which are essential for mass production.

Keywords advanced characterization, casting, nonferrous metals

1. Introduction

The increasing weight of new generation vehicles and government legislation to reduce CO_2 emissions and fuel consumption has led to a growing interest in light-weight structural materials, in general and magnesium alloys, in particular (Ref 1, 2). However, conventional Mg alloys such as AZ91D, AM60, AS41, and AE42 failed to address the updated technical demands. This mainly relates to high-temperature applications such as automotive transfer cases, cylinder head covers, intake manifold, oil pans, and engine blocks. Hence, to address the current limitations of conventional Mg alloys, various alloy development programs were initiated (Ref 3-9). The main target of these initiatives was to develop new Mg alloys with improved creep resistance. In addition, the alloys had to be die castable for mass production applications. It was evident that increasing the creep resistance usually resulted in reduced castability (Ref 10). This problem has attracted major R&D efforts and in practice was addressed by modifying the Mg alloy compositions. A good example of such alloy modification could be seen in the latest BMW development of a six cylinder Mg-Al crankcase (Ref 11). In this example, the original Mg alloy type AJ52X was replaced by AJ62X to obtain improved castability and adequate casting process of the crankcase.

The aim of the present article is to systematically evaluate the effect of wall thickness of die-cast specimens made from MRI 230D on their mechanical properties. For reference assessment, the results obtained for MRI 230D were compared to AZ91D Mg alloy. AZ91D was selected as a reference alloy due to its superior die-casting characteristics which ranks it as one of the best Mg alloy for die-casting operations.

Eli Aghion and **Amir Arnon**, Department of Materials Engineering, Ben Gurion University, Beer-Sheva, Israel; and **Nir Moscovitch**, Magnesium Research Institute, Beer-Sheva, Israel. Contact e-mails: arnonami@bgu.ac.il and egyon@bgu.ac.il.

2. Experimental

The chemical composition of MRI 230D Mg alloy was within the composition range of Dead sea Magnesium patent (Ref 12) and the main alloying elements are: aluminum, calcium, and strontium with the following composition (in wt.%): 6.6 Al, 2.5 Ca, 0.25 Sr, 0.4 Mn and up to 300 ppm Si, 30 ppm Cu, 10 ppm Ni, and 40 ppm Fe. Hence, apart from the special addition of Ca and Sr, the alloy maintained a composition within the range between AM50A and AZ91D die-cast Mg alloys. This has ensured the presence of adequate levels of Al to provide the necessary castability for die-casting procedures. The chemical composition of the reference AZ91D alloy (in wt.%): 9 Al, 0.3 Mn, 0.6 Zn and up to 500 ppm Si, 250 ppm Cu, 10 ppm Ni, and 40 ppm Fe.

Tensile properties and solidification analysis were carried out on separate die-cast tensile specimens having a rectangular cross-section with gage length of 200 mm and width of 12 mm. The thicknesses of the various specimens were: 1.5, 3, 6, 9, and 12 mm and they were cast in a multisample cavity as presented in Fig. 1. All the specimens were designed according to ASTM standards and produced using an IDRA OL-320 cold chamber die-cast machine. To ensure the soundness of the specimens, they were tested using an X-ray radiography facility having a Seifert Eresco 200 MF constant potential X-ray tube. The criterion used to distinguish between sound specimens and unacceptable specimens was their porosity content after die casting. According to this criteria, the maximum allowable porosity for specimens with thickness of up to 3 mm was 3%, for specimens over 3 mm and up to 9 mm was 2%, and for specimens above 9 mm the allowable porosity was 1.5% only.

The optimal die-casting injection values, temperatures, and lubrication parameters used for the production of MRI230D and AZ91D specimens are presented in Table 1 and 2, respectively. The solidification characteristics including mold filling were obtained using standard MAGMA simulation software (MAGMASOFT®). This was carried out mainly to determine the solidification time and rate, which are imperative to identify adequate die-casting parameters for MRI 230D alloy.

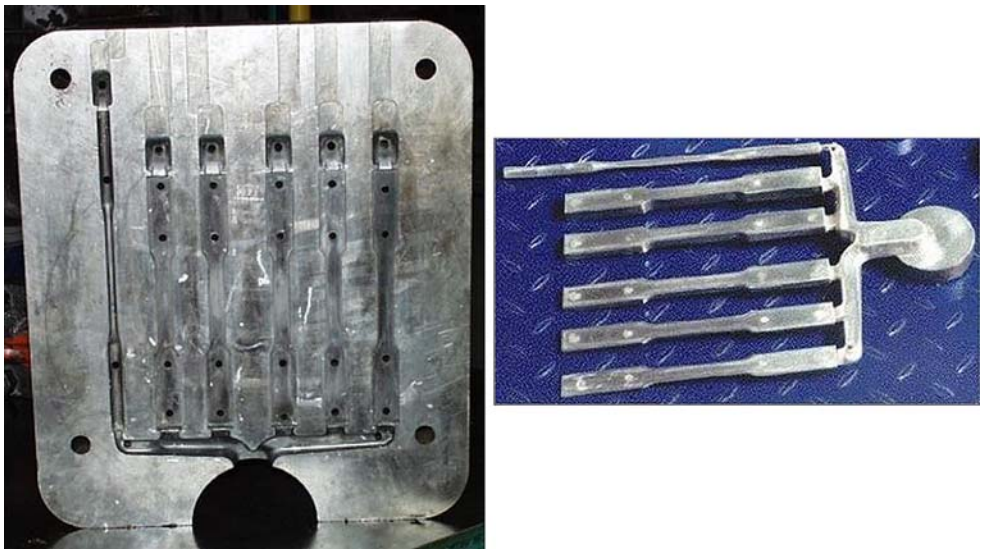

Fig. 1 Die-casting cavity and die-cast specimens

Table 1 Die-casting injection parameters used for both MRI 230D and AZ91D alloys

Parameter	
Cavity filling time	10, ms
1st phase velocity	2.2, m/s
2nd phase velocity	7.5, m/s
Shot sleeve diameter	50, mm
Shot sleeve length	400, mm

Table 2 Temperature and lubrication data used in the die casting of the specimens

	Temperature data, °C		Spraying and lubrication		
Mg alloy	Melt	Die	Spraying time, %	Mixing ratio	Dwell time, %
AZ91D	650-670	150-200	100	1/40-1/80	100
MRI230D	680-690	200-250	150-170	1/15-1/40	50-75

3. Results and Discussion

The physical and mechanical properties of MRI 230D in comparison with conventional AZ91D alloy are shown in Table 3 and 4, respectively. In terms of the physical properties, it was evident that there are some differences in the thermal characteristics and solidification range between MRI 230D and AZ91D alloy. These differences can, accordingly, affect the selection of the die-casting parameters. The differences in the thermal conductivity between MRI 230D and AZ91D can be used as an advantage in applications requiring improved heat dissipation capability. This mainly relates to the fact that the thermal conductivity of MRI 230D is about 51% higher than that of AZ91D. Evaluation of the mechanical properties revealed that MRI 230D and AZ91D are relatively similar at room temperature. However, at elevated temperatures, there

Table 3 Physical properties of MRI 230D and AZ91D

Property	MRI 230D	AZ91D
Density at 20 °C, g/cm^3	1.8	1.81
Lin. thermal exp. coeff., μm/mK	25.1	26.0
Thermal conductivity at 20 °C, W/Km	77	51
Specific heat, kJ/kg K	1.04	1.02
Nonequilibrium solidification range, °C	522-603	434-598

Table 4 Mechanical properties of MRI 230D and AZ91D

Property	MRI 230D	AZ91D
UTS at 20 °C, MPa	235	260
UTS at 150 °C, MPa	205	160
YTS at 20 °C, MPa	180	160
YTS at 150 °C, MPa	150	105
Elongation at 20 °C, %	5	6
Elongation at 150 °C, %	110	100

was a significant difference in the yield strength and ultimate tensile strength between the two alloys. In both cases, MRI 230D maintained higher strength of about 50 MPa compared to AZ91D.

The differences in the high-temperature performance between MRI 230D and AZ91D can be attributed to the variations in their chemical composition and microstructure. This is clearly illustrated in Fig. 2, showing extensive presence of Al-Ca-Sn base precipitates at grain boundaries of MRI 230D. These precipitates replace the low-melting β phase ($Mg_{17}Al_{12}$) which becomes quite soft at a relatively low temperature (around 100 °C) and cause degradation strength of the creep resistance at temperatures above 120 °C. In addition, the fact that MRI 230D has a relatively reduced quantity of Al compared to AZ91D also limits the formation of the β phase and, consequently, results in improved high-temperature strength.

Relating to the solidification characteristics, Fig. 3-5 illustrates the correlation between the mechanical properties and

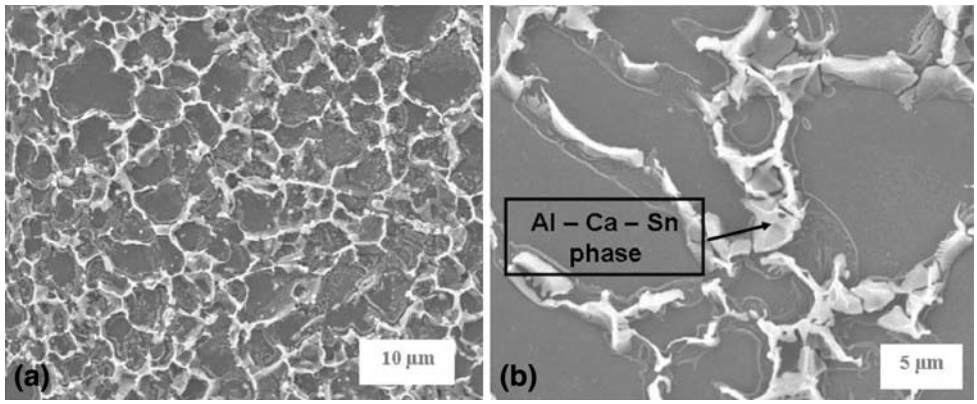

Fig. 2 Typical microstructure of MRI 230D

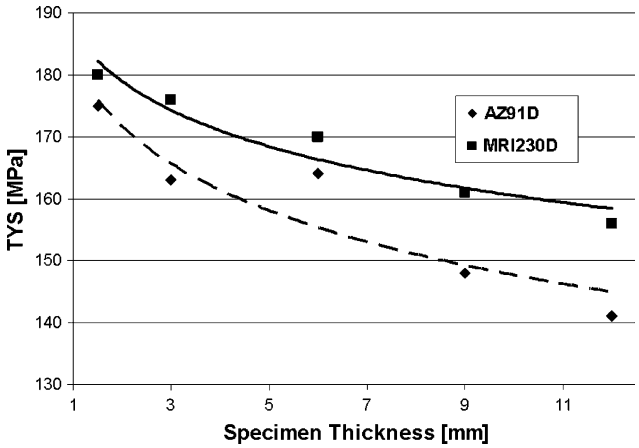

Fig. 3 Yield strength versus tensile specimen thickness for MRI 230D and AZ91D

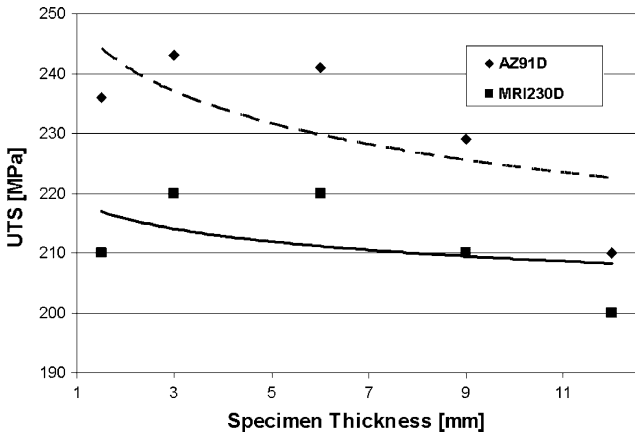

Fig. 4 Ultimate tensile strength versus specimen thickness for MRI 230D and AZ91D

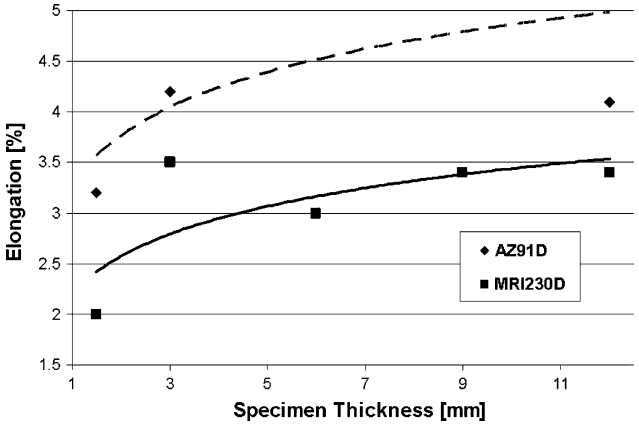

Fig. 5 Elongation versus specimen thickness for MRI 230D and AZ91D

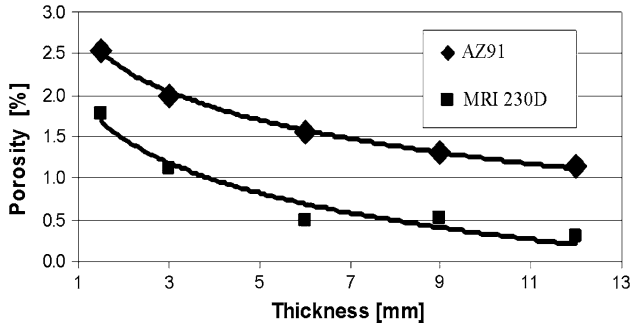

Fig. 6 The correlation between porosity levels and specimen thickness for MRI 230D and AZ91D

tensile specimen thicknesses. This clearly demonstrated that the normal drop in yield strength and ultimate tensile strength parallel to the increase in ductility obtained with AZ91D was also experienced with MRI 230D alloy. Parallel results were also obtained in terms of porosity as illustrated by the correlation between the porosity level and specimen thickness for the two alloys as shown in Fig. 6. This has revealed that the porosity in both alloys was reduced in a similar way as the wall thickness is increased due to improved solidification conditions. The relatively reduced porosity in MRI 230D compared to AZ91D is mainly related to the selection of the shot sleeve temperature. The reduced amount of Al in MRI 230 as well as the presence of Ca and Sr in this alloy results in significantly reducing the overall castability of this alloy compared to AZ91D. Hence, the optimized shot sleeve temperature for MRI 230D has to be higher than that of AZ91D. Consequently, the

increased shot sleeve temperature for MRI 230D has delayed early solidification that can cause increased amount of porosity. The similar mechanical behavior of the two alloys can be explained in light of the variation in their grain size which correlates with the specimen's thicknesses as shown in Fig. 7. According to this figure and the Hall-Petch equation, increasing the specimen thickness results in increased grain size and, subsequently, reduced strength and increased ductility.

The solidification time in terms of cooling curves and the solidification rate versus grain size obtained by using MAGMASOFT® simulation for MRI 230D and AZ91D are shown in Fig. 8 and 9, respectively. Due to the smaller nonequilibrium solidification range, the solidification time for the MRI 230D is significantly shorter compared to the AZ91D alloy. This may cause the formation of typical HPDC defects such as hot tearing. In practice it was evident that the tendency to hot tearing in MRI 230D was reduced when the die temperature was higher. This observation comes in line with the findings of Thomson et al. (Ref 13). In addition, shorter solidification time is probably related to the finer microstructure

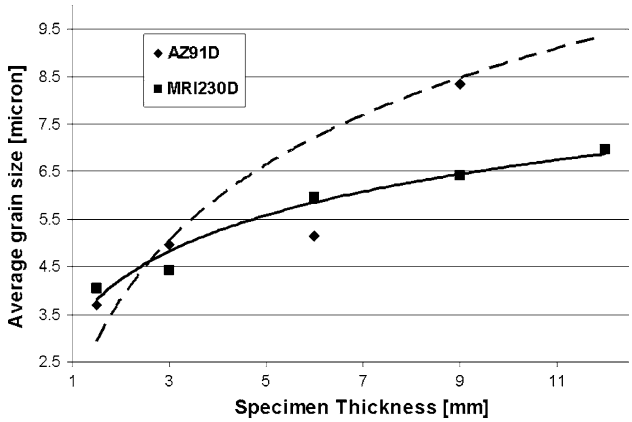

Fig. 7 The correlation between average grain size and specimen thickness for MRI 230D and AZ91D

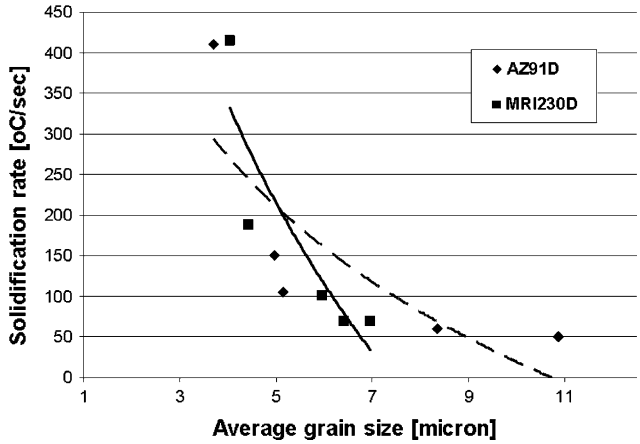

Fig. 9 The correlation between average grain size and solidification rate for MRI 230D and AZ91D

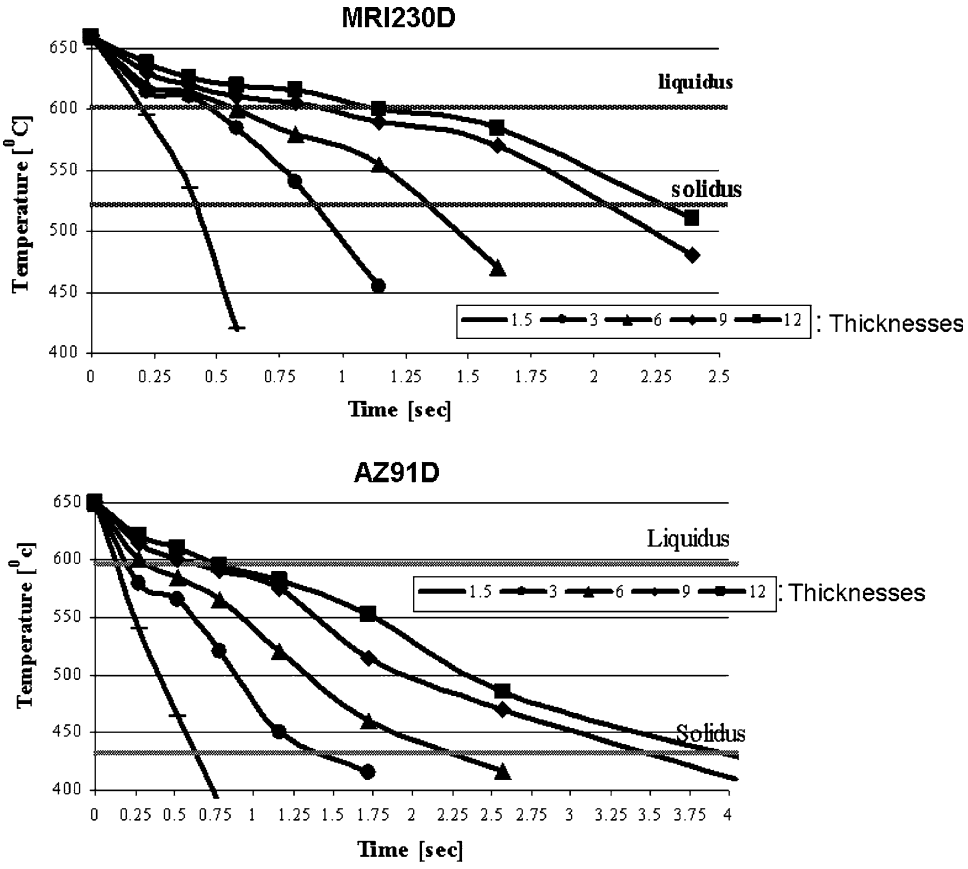

Fig. 8 Cooling curves of MRI 230D and AZ91D according to specimen thickness as obtained from MAGMASOFT® simulation

obtained for the MRI 230D alloy, in terms of grain size and distribution, in comparison to AZ91D alloy. This fact helps to maintain adequate levels of room temperature mechanical properties even though the Al content in the alloy was significantly reduced.

4. Conclusions

The results obtained by the present study demonstrate that the differences in wall thickness of MRI 230D die-cast specimens affect their solidification rate characteristics. The reduced solidification rate obtained in thicker specimens resulted in increased grain size and reduced TYS and UTS while increasing %El. In terms of porosity, thicker specimens tend to form shrink porosity while thinner specimens tend to form gas porosity. The gas porosity is mainly related to the atomized flow pattern of the molten metal that occurs in thinner specimens.

In general, the modifications in the mechanical properties of MRI 230D specimens due to the differences in wall thickness was similarly observed also in AZ91D alloy. However, it should be pointed out that the porosity level in MRI 230D was reduced compared to the porosity obtained in AZ91D. This was due to the higher shot sleeve temperature that was used for MRI 230D. Higher temperature in the shot sleeve delays early solidification and, consequently, reduces the level of porosity in the cast specimen.

References

1. G. Simonds and B. Su, Magnesium in Automobiles Application Trends and Advantages, *IMA 63rd Annual World Magnesium Conference*, May 21-24, 2006 (Beijing, China), p 66–72
2. K. Jereza, R. Brindle, S. Robison, J.N. Hryn, D.J. Weiss, and B.M. Cox, The Road to 2020: Overview of the Magnesium Casting Industry Technology Roadmap, *Magnesium Technology 2006, TMS Annual Meeting*, March 12-16, 2006 (San Antonio, TX), p 89–94
3. H. Westengen, P. Bakke, J.I. Skar, and H. Gjestland, New Magnesium Die Casting Alloys: Driving Development of Critical Automotive Applications, *IMA 63rd Annual World Magnesium Conference*, May 21-24, 2006 (Beijing, China), p 34–42
4. M.O. Pekguleryuz and A.A. Kaya, Magnesium Die-Casting Alloys for High Temperature Applications, *Magnesium Technology 2004*, *TMS Annual Meeting*, March 2004 (Charlotte, NC), p 281–287
5. G.L. Dunlop, T. Abbot, M. Murray, C.J. Bettles, and MA Gibson, New Magnesium Diecasting Alloys for Decorative and Powertrain Applications, *IMA 63rd Annual World Magnesium Conference*, May 21-24, 2006 (Beijing, China), p 26–33
6. E. Aghion, N. Moskovitch, and A. Arnon, Solidification Characteristics of Newly Developed Die Cast Magnesium Alloy MRI153M, *Mater. Sci. Technol.*, 2007, **23**(3), p 270–275
7. L. Cisar, Y. Yoshida, S. Kamado, Y. Kojima, and F. Watanabe, Development of High Strength and Ductile Magnesium Alloys for Automobile Applications, *Mater. Sci. Forum*, 2003, **419–422**, p 249–254
8. K. Ozturk, Y. Zhong, A.A. Luo, and Z.K. Liu, Creep Resistant Mg-Al-Ca Alloys: Computational Thermodynamics and Experimental Investigation, *JOM*, 2003, **55**, p 40–44
9. J. Göken, J. Bohlen, N. Hort, D. Letzig, and K. U. Kainer, New Development in Magnesium Technology for Light Weight Structures in Transportation Industries, *Mater. Sci. Forum*, 2003, **426–432**, p 153–162
10. E. Aghion, B. Bronfin, F. Von Buch, S. Schumann, and H. Friedrich, Dead Sea Magnesium Alloys Newly Developed for High Temperature Applications, *Magnesium Technology 2003, TMS Annual Meeting*, March 2-6, 2003 (San Diego, CA), p 177–182
11. A. Fischersworring-Bunk, C. Landerl, A. Fent, and J. Wolf, The New BMW Inline Six-Cylinder Composite Mg/Al Crankcase, *IMA 62nd Annual World Magnesium Conference*, May 22-24, 2005 (Berlin, Germany), p 51–60
12. B. Bronfin, E. Aghion, V. Von Buch, S. Schumann, and M. Katzer, High Strength Creep Resistant Magnesium Alloys, US Patent 7041179, 2006
13. J.P. Thomson, M. Sodayappam, and M. Sahoo, Evaluation of the Hot Tearing Susceptibility of Selected Mg Casting Alloys in Permanent Molds, *International Conference on Magnesium Alloys and their Applications* (Dresden, Germany), 2006, p 234–239